Hox5 genes direct elastin network formation during alveologenesis by regulating myofibroblast adhesion

Steven M. Hrycaj[a], Leilani Marty-Santos[a], Cristina Cebrian[b,c], Andrew J. Rasky[d], Catherine Ptaschinski[d], Nicholas W. Lukacs[d], and Deneen M. Wellik[a,1]

[a]Department of Internal Medicine, Division of Genetic Medicine, University of Michigan, Ann Arbor, MI 48109-2200; [b]Department of Internal Medicine, Division of Gastroenterology, University of Michigan, Ann Arbor, MI 48109-2200; [c]Division of Developmental Biology, Cincinnati Children's Hospital Medical Center, Cincinnati, OH 45229; and [d]Department of Pathology, University of Michigan, Ann Arbor, MI 48109

Edited by Brigid L. M. Hogan, Duke University Medical Center, Durham, NC, and approved September 27, 2018 (received for review April 24, 2018)

***Hox5* genes (*Hoxa5*, *Hoxb5*, *Hoxc5*) are exclusively expressed in the lung mesenchyme during embryogenesis, and the most severe phenotypes result from constitutive loss of function of all three genes. Because *Hox5* triple null mutants exhibit perinatal lethality, the contribution of this paralogous group to postembryonic lung development is unknown. Intriguingly, expression of all three *Hox5* genes peaks during the first 2 weeks after birth, reaching levels far exceeding those measured at embryonic stages, and surviving *Hoxa5* single and *Hox5 AabbCc* compound mutants exhibit defects in the localization of alveolar myofibroblasts. To define the contribution of the entire *Hox5* paralogous group to this process, we generated an *Hoxa5* conditional allele to use with our existing null alleles for *Hoxb5* and *Hoxc5*. Postnatally, mesenchymal deletion of *Hoxa5* in an *Hoxb5/Hoxc5* double-mutant background results in severe alveolar simplification. The elastin network required for alveolar formation is dramatically disrupted in *Hox5* triple mutants, while the basal lamina, interstitial matrix, and fibronectin are normal. Alveolar myofibroblasts remain Pdgfrα+/SMA+ double positive and present in normal numbers, indicating that the irregular elastin network is not due to fibroblast differentiation defects. Rather, we observe that SMA+ myofibroblasts of *Hox5* triple mutants are morphologically abnormal both in vivo and in vitro with highly reduced adherence to fibronectin. This loss of adhesion is a result of loss of the integrin heterodimer Itga5b1 in mutant fibroblasts. Collectively, these data show an important role for *Hox5* genes in lung fibroblast adhesion necessary for proper elastin network formation during alveologenesis.**

Hox5 | alveologenesis | elastin network | distal lung fibroblasts | integrin regulation

Mammals have 39 *Hox* genes that can be further categorized into 13 paralogous groups based on sequence similarity, position within the cluster, and displaying the most similar expression patterns during embryogenesis (1). Genetic studies have shown that *Hox* paralogs function redundantly in many aspects of organogenesis (2–16). While classically considered embryonic patterning regulators, accumulating evidence supports a continued role for *Hox* genes during postnatal development and adult homeostasis (17–25). A limitation of studying postnatal *Hox* function is that mutations for entire paralogous groups often lead to embryonic lethality (6–8, 14, 26–30). As a result, previous studies on postembryonic and adult functions of *Hox* genes have mainly relied on analyzing surviving compound mutant animals. While these studies are informative, an important caveat of these experiments is that the retention of WT alleles may be significantly compensating for defects that would be revealed from complete loss of *Hox* function.

Alveologenesis is the final stage of lung development. During this phase, the saccules are subdivided into alveoli, which maximizes the gas exchange surface area of the distal lung. Disruptions in alveologenesis are common in humans and result in alveolar simplification (fewer and larger alveoli), a hallmark of bronchopulmonary dysplasia (BPD). One critical event required for alveologenesis is the generation, modeling, and remodeling of an elastin-based ECM. This elastin-based matrix provides the complex, net-like structure mechanically required for alveolar formation and for the stretch and recoil crucial for breathing. SMA+ myofibroblasts have been historically attributed as the cells responsible for elastin production; however, it has recently been shown that a nascent elastin network is present in the distal lung by embryonic day 18.5 (E18.5), several days before the onset of alveologenesis or the detection of SMA in the distal lung (31). These data indicate that even our most basic understanding of alveologenesis requires clarification.

We have previously reported that all three *Hox5* genes are exclusively expressed in the lung mesenchyme and that loss of function of all three genes leads to severe early developmental lung defects and perinatal death (7). Additional analyses using constitutive null alleles reveal that, while *Hox5 AAbbcc* animals are viable and phenotypically normal at newborn stages, *Hoxa5* single-mutant animals exhibit developmental lung defects that result in perinatal lethality (7, 32). These data provide functional evidence that *Hoxa5* provide a larger contribution to phenotype compared with both *Hoxb5* and *Hoxc5*. We also previously reported that compound *Hox5* mutant mice (*Hox5 AabbCc*) are viable and phenotypically normal at birth; however, they develop alveolar simplification at postnatal stages coincident with abnormal SMA+ myofibroblast localization in the distal airway, consistent with redundant functional roles during postembryonic lung development (33). To pursue these questions, we generated

Significance

***Hox5* genes play critical roles in embryonic lung development, but mutants die at birth, preventing investigation of potential postnatal functions for these genes. Surprisingly, we show that the highest expression levels of *Hox5* genes occur 1–2 weeks after birth. We created a conditional allele for *Hoxa5* that allowed us to generate and study mutants for all three *Hox5* genes during postnatal development. *Hox5* mutants have poorly developed alveoli and expanded distal airspaces resulting from an abrogated elastin network. These defects arise from the inability of *Hox5* mutant fibroblasts to adhere to the fibronectin matrix due to loss of integrins Itga5/b1. Thus, our data highlight redundant roles for all three *Hox5* genes in regulating fibroblast adhesion and elastogenesis during alveologenesis.**

Author contributions: S.M.H. and D.M.W. designed research; S.M.H., L.M.-S., C.C., A.J.R., C.P., and N.W.L. performed research; S.M.H. and C.C. contributed new reagents/analytic tools; S.M.H., L.M.-S., N.W.L., and D.M.W. analyzed data; and S.M.H. and D.M.W. wrote the paper.

The authors declare no conflict of interest.

This article is a PNAS Direct Submission.

[1]To whom correspondence should be addressed. Email: dwellik@umich.edu.

This article contains supporting information online at www.pnas.org/lookup/suppl/doi:10.1073/pnas.1807067115/-/DCSupplemental.

Published online October 22, 2018.

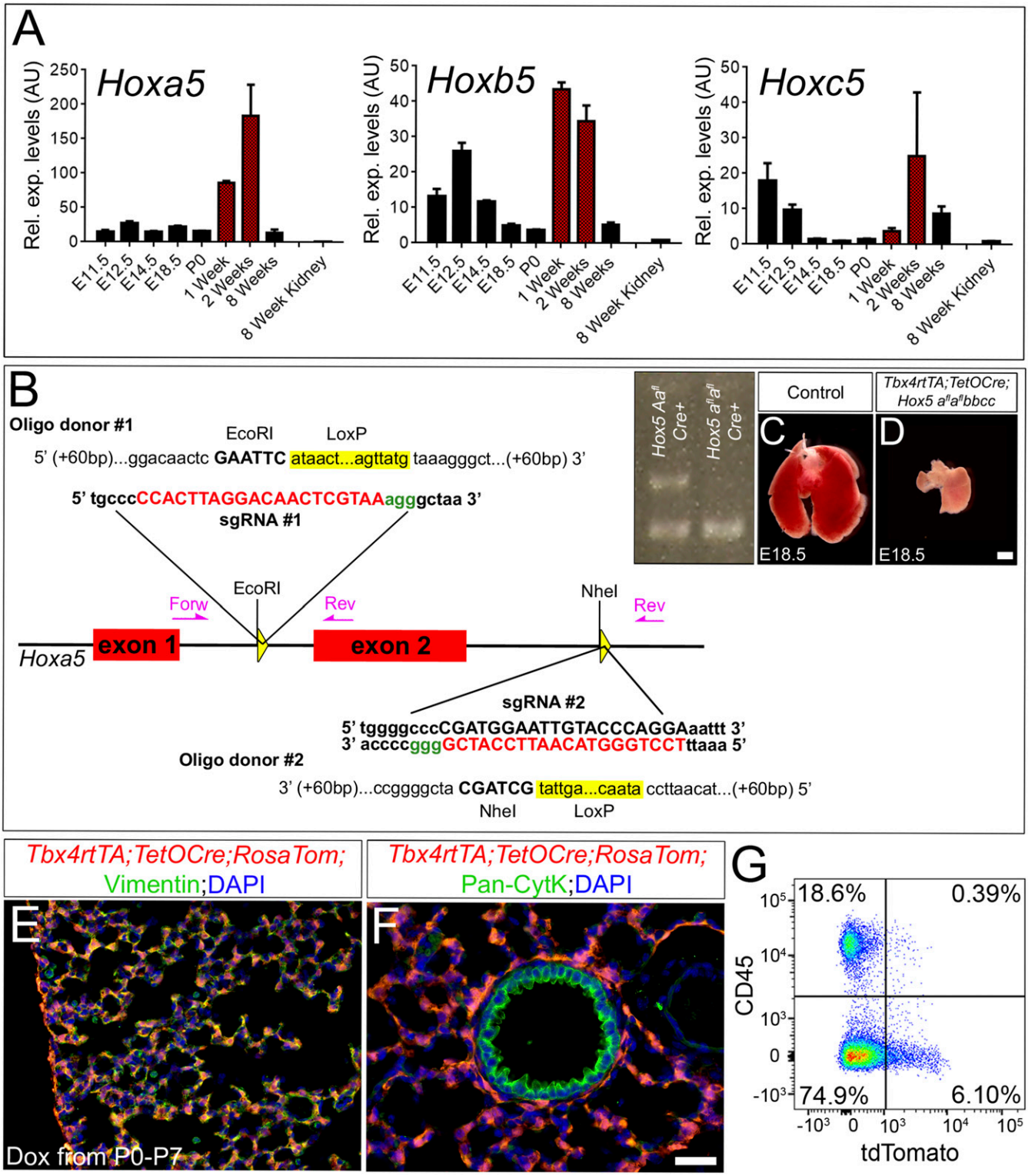

Fig. 1. qPCR expression profile of *Hoxa5*, *Hoxb5*, and *Hoxc5* through developmental, postnatal, and adult stages showing highest up-regulation of expression at early postnatal stages (*A*). Generation of *Hoxa5* conditional allele. Diagram outlining two successive rounds of targeting into zygotes to generate insertion of the two LoxP sites. Correct targeting was confirmed by PCR and sequencing. Primers used to detect each LoxP site and the deleted allele are shown with pink arrows. Example PCR genotyping for intronic LoxP site (*B*). Targeting in *cis* was confirmed by cotransmission through the germline. Phenotype from early (E9.5) deletion of *Tbx4rtTA;TetOCre;Hox5 a^{fl}a^{fl}bbcc* phenocopy null loss-of-function lung phenotypes (*C* and *D*). (Scale bar: 1.0 mm.) Mesenchyme-specific deletion is efficiently enacted by *Tbx4rtTA;TetOCre*. Lung sections from P7 *Tbx4rtTA;TetOCre;ROSA26-LSL-tdTomato* animals dosed with Dox from P0 to P7 show significant coexpression of RosaTOM (red) with a marker of mesenchyme (vimentin; green) and no overlap with an epithelial marker (pancytokeratin; green) (*E* and *F*). (Scale bar: 50 μm.) Flow cytometry showing that all tdTomato+ cells are exclusively found in the nonhematopoietic (CD45−) population (*G*).

a conditional *Hoxa5* allele to use in combination with existing null alleles for *Hoxb5* and to study the roles of all three *Hox5* genes during postnatal development. To delete *Hoxa5* function exclusively in the lung mesenchyme, we used a previously reported *Tbx4rtTA*;*TetOCre* allele that has been shown to be specific to this cell population (34). Conditional deletion of *Hoxa5* alone results in alveolar simplification. However, the alveolar simplification phenotype of *Hoxa5* is greatly exacerbated with the addition of null alleles for *Hoxb5* and *Hoxc5* and provides evidence that all three *Hox5* genes are required for proper alveolar development. Despite the severe alveolar expansion, major components of the ECM, including the basal lamina, collagen interstitial matrix, and fibronectin, are unaffected in conditional *Hox5* triple mutants. However, the normally elaborate, interconnected elastin network is highly perturbed. SMA/Pdgfrα double-positive myofibroblasts are present in normal numbers in mutant lungs but are morphologically abnormal both in vivo and in vitro. We show that cultured SMA+ fibroblasts from mutant lungs exhibit reduced adhesion to fibronectin, a cellular phenotype that is also observed in vivo. This phenotype correlates with loss of Itgα5/β1 integrin expression in lung fibroblasts, and blocking antibodies to these integrins leads to a similar phenotype in WT cells in vitro. Collectively, these data indicate that mesenchymal *Hox5* genes direct the proper formation of the elastin network by integrin-regulated myofibroblast adherence to the distal lung ECM.

Results

***Hox5* Genes Exhibit Highest Levels of Expression During Early Postnatal Stages.** All three *Hox5* genes are exclusively expressed in the lung mesenchyme developmentally (and not epithelium), and constitutive loss of function of all three *Hox5* genes leads to severe, early embryonic lung defects and 100% neonatal lethality (7). As expression of all three *Hox5* genes decreases in the lung during embryogenesis (Fig. 1*A*), we first examined whether these genes were expressed during postnatal development. Unexpectedly, qPCR analyses reveal that the expression levels of all three *Hox5* genes peak during alveologenesis stages, 1–2 wk after birth, reaching significantly higher expression levels than observed at any embryonic developmental stage (Fig. 1*A*). These data provide compelling evidence that all three *Hox5* paralogous genes might play direct roles in alveologenesis.

Generation of *Hoxa5* Conditional Allele. A caveat of analyzing compound loss-of-function *Hox5 AabbCc* mutants is that the retention of two WT alleles during postnatal stages may be compensating for defects that would be revealed from complete loss of *Hox5* paralogous function. However, animals that are only null for *Hoxa5* exhibit perinatal lethality (7, 32). To circumvent this limitation, we used CRISPR/Cas9 technology to generate a conditional *Hoxa5* allele in which exon 2 (which encodes the DNA-binding homeodomain) is flanked by *LoxP* sites. Using our existing null alleles for *Hoxb5* and *Hoxc5* and the newly generated conditional allele for *Hoxa5*, we enacted recombination at E9.5 using *ROSA-CreERT2* (35) and show a complete deletion at the *Hoxa5* locus (Fig. 1*B*). Because all three *Hox5* paralogs are exclusively expressed in the lung mesenchyme (7), we used a previously reported *Tbx4rtTA*;*TetOCre* driver line that expresses Cre in response to doxycycline (Dox) and reports efficient and exclusive deletion in lung mesenchyme during developmental, postnatal, and adult stages (34). Deletion enacted with Dox treatment from E9.5 to E18.5 using*Tbx4rtTA*;*TetOCre* leads to a recapitulation of our previously reported *Hox5* triple null phenotype (Fig. 1 *C* and *D*), validating our conditional allele. The *Tbx4rtTA*;*TetOCre* embryonic deletion also confirms that *Hox* function in the developing embryonic lung is restricted to lung mesenchyme as the expression suggests.

***Hox5* Conditional Triple-Mutant Lungs Exhibit the Most Severe Distal Lung Phenotypes.** It has been reported that alveologenesis initiates at approximately postnatal day 4 (P4), peaks during the first 2 wk of life, and ends 4–5 wk after birth in mice (31, 36, 37). To determine efficiency of the *Tbx4* transgene in enacting recombination at postnatal stages, we treated *Tbx4rtTA*;*TetOCre*;*ROSA-LSL-tdTomato* animals with Dox in the drinking water beginning at P0 and analyzed the lung tissue at P7 (38). Costaining lungs from these mice with antibodies to either vimentin or pancytokeratin to specifically mark the lung mesenchyme or epithelium, respectively, reveals a nearly complete overlap of tdTomato expression with vimentin-positive mesenchyme and no coexpression with pancytokeratin-positive epithelium (Fig. 1 *E* and *F*). Additionally, flow cytometry analysis shows that there is no Cre-induced recombination (tdTomato+) in hematopoietic cells (Fig. 1*G*). These data collectively indicate that our postnatal Dox dosing strategy at postnatal stages is efficient and specific to the lung mesenchyme.

Using this strategy, we examined conditional loss of function of *Hoxa5* at postnatal stages alone and in combination with our existing null alleles for *Hoxb5* and *Hoxc5* to determine the allelic contribution to postnatal phenotypes. After P0–P7 Dox treatment, mean alveolar chord length measurements at P7 show that mice carrying only the *Hoxa5* conditional allele with no Cre result in no phenotype (Fig. 2*D*). *Hox5 AAbbcc* null mutants have only a mild alveologenesis phenotype (~11% increase in mean alveolar chord length) and are identical to *Hox5* $a^{fl}a^{fl}$*bbcc* mice in the absence of Cre (Fig. 2*D*). These data show that our *Hoxa5* conditional allele does not contribute to phenotype in the absence of Cre and functions as a WT *Hoxa5* allele. In contrast, *Tbx4rtTA*;*TetOCre*;*Hox5* $a^{fl}a^{fl}$*BBCC* Dox-treated animals (*Hoxa5* single conditional mutants) exhibit alveolar simplification with increased mean alveolar chord length measurements (~27% increase compared with WT animals) (Fig. 2*D*). Thus, conditional loss of *Hoxa5* function alone provides a much larger contribution to postnatal lung phenotypes than *Hoxb5*/*Hoxc5* double mutants. Compound four-allele *Hox5* null mutant animals of the genotype *Hox5 AabbCc* show an ~38% increase in mean alveolar chord length, suggesting redundancy of function

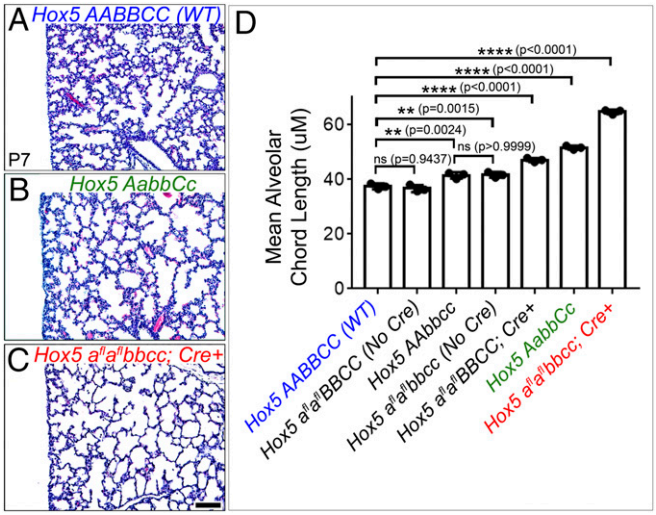

Fig. 2. Allelic series of alveolar phenotypes. Representative H&E sections through P7 WT (*A*), *Hox5* four-allele (*B*), and conditional triple mutants (Dox from P0 to P7) (*C*). (Scale bar: 100 μm.) Mean alveolar chord length values for each genotype are shown in *D*. Values are the mean measurement of every vertical and horizontal grid cross-line of four random 20× images from each animal measured; $n = 3$ animals from each group were measured. *P* values and statistical significance were determined by an unpaired Student's *t* test. Asterisks denote statistical significance; ns, not significant (*D*).

of all three *Hox5* paralogs during early postembryonic lung development (Fig. 2 *A*, *B*, and *D*). Consistent with this, conditional deletion of *Hoxa5* in an *Hoxb5*/*Hoxc5* null background (*Hox5* triple mutants) results in the most severe dilation of the distal airway, evidenced by an ∼73% increase in mean alveolar chord length compared with the WT, significantly more severe that any partial mutant phenotype (Fig. 2). Additionally, we show that this phenotype does not simply represent a delay in alveolar development, as alveolar simplification is still observed at 4 wk of age (*SI Appendix*, Fig. S1). These data further reinforce that all three *Hox5* paralogs are functionally redundant during postnatal lung development. We, therefore, focused the remainder of our analysis on conditional *Hox5* triple-mutant animals (*Tbx4rtTA*;*TetOCre*;*Hox5* $a^{fl}a^{fl}bbcc$).

The Enlarged Distal Lung Phenotypes of Conditional *Hox5* Triple Mutants Result in Increased Lung Compliance and Decrease Elastance. To examine whether the observed histological changes result in altered lung physiology at adult stages, we performed invasive pulmonary functional testing (pulmonary maneuvers) on 10-wk control and *Hox5* conditional mutants in which *Hoxa5* function was deleted with Dox treatment from P0 to P14. Increased lung volumes of conditional *Hox5* mutants are indicated by significant increases in inspiratory capacity (IC), vital capacity (VC), forced vital capacity (FVC), and forced expiratory volume (FEV) (Fig. 3 *A*–*D*). Additionally, *Hox5* mutants show increased lung compliance as determined by significant increases in chord compliance (Cchord), compliance at zero pressure (Cp0), and peak compliance (Cpk) and a significant decrease in lung elastance (Fig. 3 *E*–*H*). Thus, the alveologenesis defects in *Hox5* mutants result in severe physiological changes in adult lung function parameters.

Conditional *Hox5* Triple-Mutant Phenotypes Do Not Result from Aberrant Mesenchymal Canonical Wnt Signaling. At embryonic stages, we have previously shown that *Hox5* genes direct proper lung growth, branching, and patterning by regulating *Wnt2*/*2b* expression in the lung mesenchyme (7). A recent study reports that, while conditional deletion of canonical Wnt/β-catenin signaling in AT2 cells using an $Sftpc^{CreErt2}$ allele from P4 to P30 results in decreased numbers of AT2 cells, the gross morphology of the distal lung is unaffected, with no observed alveolar simplification defects (39). To test for potential activity in the lung mesenchyme as well, we generated *Tbx4rtTA*;*TetOCre*;*β-Cat*$^{fl/fl}$ to determine if conditional inactivation of canonical Wnt/β-catenin signaling specifically in the lung mesenchyme could recapitulate the phenotypes observed in conditional *Hox5* triple mutant postnatally. Histological analyses of P7 lungs from *Tbx4rtTA*;*TetOCre*;*β-Cat*$^{fl/fl}$ mice that were administered Dox from P0 to P7 were indistinguishable from controls, with no differences in mean alveolar chord length measurements (*SI Appendix*, Fig. S2). Taken together, these data indicate that the severe distal airway dilation observed in conditional *Hox5* triple mutants is not attributed to aberrant canonical Wnt/β-catenin signaling in the distal lung and that *Hox5* genes are directing alveologenesis through a mechanism independent of canonical Wnt/β-catenin regulation during early postnatal development.

The Elastin-Based ECM Network Is Severely Disrupted in *Hox5* Triple-Mutant Distal Lungs. Previous studies have shown that the ECM plays a fundamental role in coordinating proper alveologenesis in the distal lung (40–45). We, therefore, analyzed several key ECM components in conditional P0–P7 Dox-treated *Hox5* triple-mutant mice and compared them with controls. Immunohistochemical immunofluorescence (IHC-IF) analyses reveal no changes in the expression patterns of basement membrane components (laminin, Col4), the collagen-based interstitial matrix (Col3), or

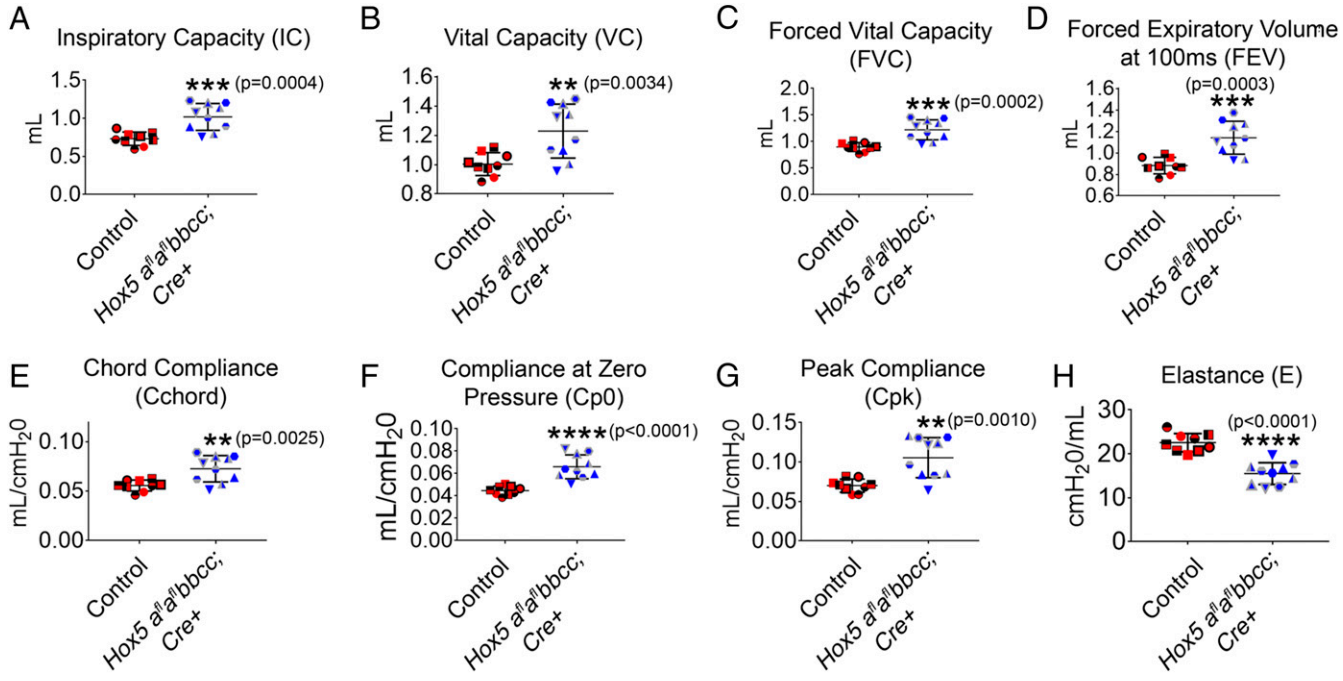

Fig. 3. Conditional *Hox5* triple mutants exhibit impaired pulmonary function at adult stages. Quasistatic and fast flow maneuvers were performed using the Buxco system to measure lung volume, compliance, and elastance in tracheotomized mice. Conditional *Hox5* mutants exhibit increased lung volume indicated by significant increases in IC (*A*), VC (*B*), FVC (*C*), and FEV (*D*). Increased lung compliance of *Hox5* mutants is shown by significant increases in Cchord (*E*), Cp0 (*F*), and Cpk (*G*). Conditional *Hox5* mutants also exhibit a significant decrease in elastance at adult stages (*H*); $n = 9$ control and $n = 10$ *Hox5* mutants were measured for PFT analyses. Individual mice are represented by a specific colored shape. *P* values and statistical significance were determined by an unpaired Student's *t* test. Asterisks denote statistical significance.

fibronectin in conditional *Hox5* triple mutants compared with controls (Fig. 4 *A*–*H*). These data are further supported by Western analyses that show no changes in distal lung protein levels of laminin, Col4, Col3, or fibronectin in conditional *Hox5* triple mutants compared with controls (Fig. 4*K*). In contrast, dramatic disruptions of the elastin-based matrix are observed in conditional *Hox5* triple mutants compared with controls by P7 (Fig. 4 *I* and *J*); 3D reconstruction analyses of 100-μm-thick lung sections reveal that the elastin network of conditional *Hox5* triple mutants is discontinuous and markedly more diffuse compared with controls by P7 after deletion at P0 (Fig. 5 *A* and *B* and Movies S1 and S2). Of note, there is no obvious change in the elastin morphology or staining in the lung vasculature (Fig. 5 *A* and *B*). Transmission EM (TEM) imaging of the alveolar septal walls confirms that the elastin network is decreased and discontinuous in *Hox5* triple mutants (Fig. 5 *C* and *D*). However, despite the dramatic disruption of the elastin-based network in conditional *Hox5* triple mutants, Western analyses reveal no changes in the total levels of soluble elastin protein (Fig. 4*K*), and qPCR analyses measure no differences in the expression levels of elastin, microfibril, or elastin-associated deposition and processing genes in *Hox5* triple mutants (*SI Appendix*, Fig. S3).

Early Establishment of the Elastin Network. Establishment of the elastin-based ECM is a critical event that is necessary for proper alveologenesis. Surprisingly, a recent report shows that an elastin fiber network already exists in the distal lung interstitium by birth, before the initiation of alveologenesis and the appearance of SMA+ fibroblasts in the distal lung (31). Our data confirm and extend these observations, and they show that elastin protein is only expressed in regions surrounding the proximal airway of the lung through E16.5 and first appears in the distal lung beginning at E17.5 (Fig. 6 *A* and *B*). The elastin network continues to be elaborated over the next several days and is significantly remodeled with fewer thinner fibers and more tightly organized elastin bundles around the alveolar openings by P7 (Fig. 6 *C*–*F*). Also, in agreement with Branchfield et al. (31), we do not observe SMA+ fibroblasts in the distal lung region until ∼P3, and we additionally confirm that SMA+ fibroblasts form tight, parallel networks with elastin by P7 (Fig. 6 *G*–*J*). Thus, our data provide important corroboration that the initial elastin network begins to form several days before the appearance of SMA+ fibroblasts in the distal lung. These data represent an important clarification of the basic anatomical state of the lung at newborn stages that needs to be considered when assessing the genetic contribution of any factor to alveologenesis, including the *Hox5* genes.

Fibroblasts Exhibit Dramatic Morphological Defects in Conditional *Hox5* Triple-Mutant Lungs. We next analyzed the distribution of fibroblasts in the distal lung during postnatal development. SMA+ fibroblasts are present in the distal lung of conditional *Hox5* triple mutants at P7; however, their morphology is strikingly different from in controls (Fig. 5 *E*–*H*). In contrast to the elongated and flattened SMA+ fibroblasts that adhere to the ECM in the developing alveoli in controls, mutant SMA+ fibroblasts in the distal lung appear small and rounded and do not extend along the ECM (Fig. 5 *E*–*H*). Despite the clear morphological defects of the SMA+ fibroblasts and the disrupted elastin network, quantification of SMA+ fibroblasts in conditional *Hox5* triple mutants reveals no differences in cell number compared with controls, and Western analyses show no changes in the overall levels of SMA protein (Fig. 5*K* and *SI Appendix*, Fig. S4). We also find that all SMA+ fibroblasts coexpress Pdgfrα in conditional *Hox5* triple mutants at P7 (Fig. 5 *I* and *J*), and quantification shows no difference in the proportion of Pdgfrα+ fibroblasts compared with controls (Fig. 5*K*), consistent with proper fibroblast differentiation during early postnatal stages.

In addition to the fibroblasts, we also examined other cell types specific to the distal lung. We find no differences in the

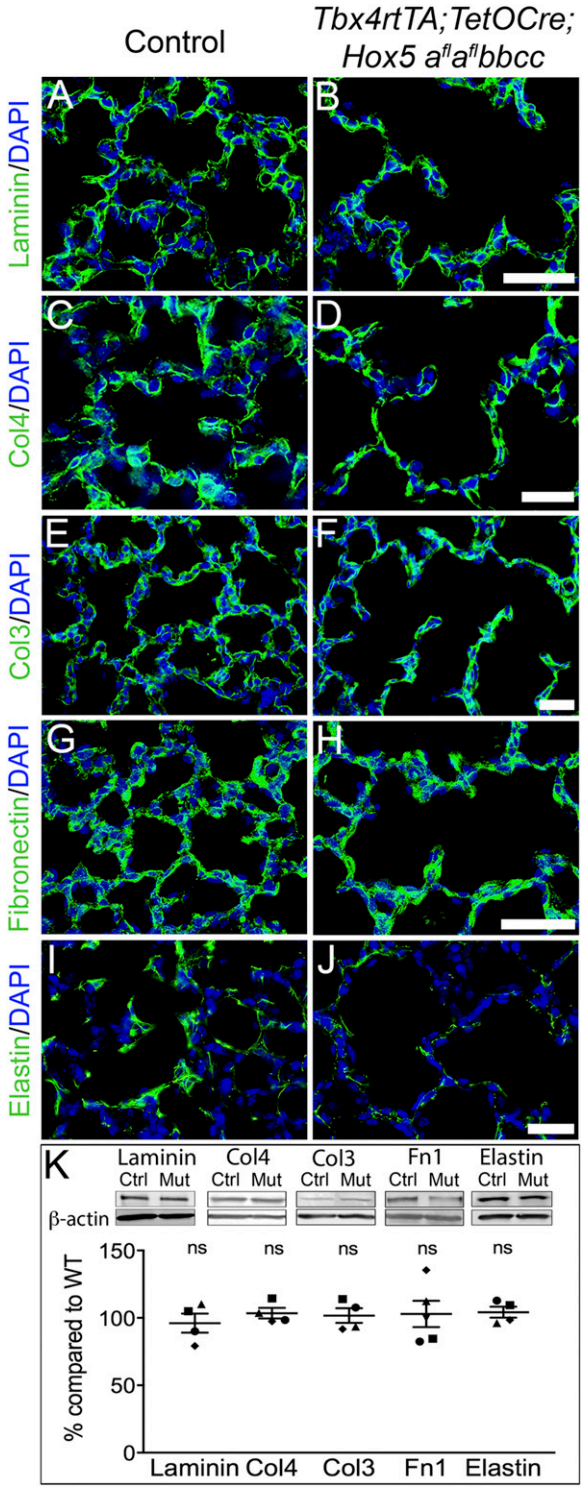

Fig. 4. Expression of major ECM components in control and *Hox5* triple mutants at P7. Immunohistochemistry reveals no major differences in the basement membrane [Laminin (*A* and *B*), Col4 (*C* and *D*)], collagen-based ECM [Col3 (*E* and *F*)], or fibronectin (*G* and *H*) in the distal lung. Expression of tropoelastin is reduced in *Hox5* triple mutants compared with control (*I* and *J*). (Scale bars: 50 μm.) Western analysis shows no differences in the protein levels of Laminin, Col4, Col3, fibronectin, or elastin between controls and *Hox5* triple mutants (*K*). ns, not significant (*K*).

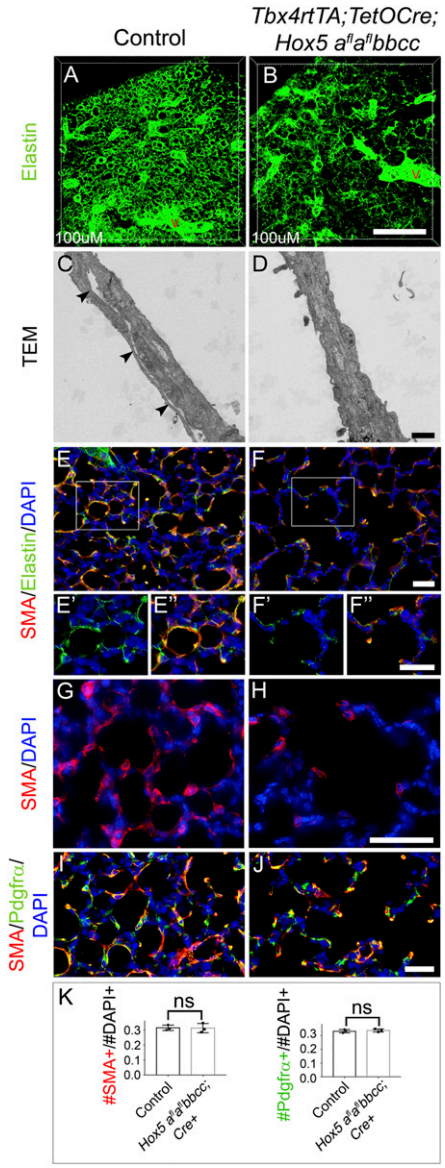

Fig. 5. Elastin and SMA networks are perturbed in *Hox5* triple mutants by P7; 3D reconstruction of 100-μm-thick vibratome sections showing the elastin network is discontinuous and diffuse in *Hox5* triple mutants compared with controls. Blood vessels in each panel are labeled with a red V (*A* and *B*). (Scale bar: 200 μm.) TEM imaging of the alveolar septal walls in WT and *Hox5* triple mutants confirms that mutants exhibit a discontinuous elastin network (*C* and *D*). Black arrowheads point to an elastin bundle in *C*. (Scale bar: 1 μm.) SMA+ myofibroblast morphology is extremely abnormal compared with controls in *Hox5* triple mutants and does not properly extend along the alveolar matrix (*E* and *F*). SMA–elastin costaining reveals that the morphologically abnormal SMA+ myofibroblasts of *Hox5* triple mutants continue to be tightly associated with the elastin network as observed in controls (*E*–*F*″). (Scale bars: 50 μm.) The 100× magnification images of the distal lung show the failure of SMA+ fibroblasts to properly extend along the ECM in *Hox5* triple mutants (*G* and *H*). (Scale bar: 200 μm.) Coexpression analyses show that *Hox5* triple-mutant SMA+ myofibroblasts continue to coexpress Pdgfrα, despite their abnormal morphology at P7 (*I* and *J*). (Scale bar: 5 μm.) Quantification (proportion of total DAPI+ cells) shows no differences in ratios of SMA+ or Pdgfrα+ cells in *Hox5* triple mutants (*K*). ns, not significant (*K*).

morphology or distribution of ADRP+ lipofibroblasts, Sftpc+ AECII cells, or Erg+ endothelial cells in conditional *Hox5* triple mutants, and quantification verifies no differences in the numbers of these cell types (Fig. 7 *A*–*F* and *K*). We observe no changes in PECAM+ endothelial cells, T1α+ AECI cells, or phalloidin staining in the distal lung in *Hox5* mutants (Fig. 7 *G*–*J* and *SI Appendix*, Fig. S5 *A* and *B*).

***Hox5* Triple-Mutant SMA+ Myofibroblasts Exhibit Decreased Adhesion to Fibronectin in Vitro.** To further explore the cellular phenotype of the lung fibroblasts, we cultured primary lung cells harvested from P7 control and *Hox5* triple-mutant animals on fibronectin-coated plates after Dox treatment of the animals from P0 to P7. Similar to what we observe in vivo, *Hox5* triple-mutant myofibroblasts exhibit abnormal morphology in vitro, lacking the normal extended cell bodies that extend along the fibronectin matrix, although they clearly express SMA and exhibit normal phalloidin staining (Fig. 8 *A* and *B* and *SI Appendix*, Figs. S5 *C*–*H* and S6). These data are consistent with an inability of these cells to properly adhere to the ECM. We performed in vitro adhesion assays on primary lung fibroblasts harvested from P7 control and *Hox5* triple mutants to test this further. Briefly, 10,000 cells were plated onto fibronectin-coated plates, allowed to adhere for 1 h, and then centrifuged upside down at low speed to remove nonadherent cells. In this assay, *Hox5* mutant cells exhibit a >35% decrease in their ability to adhere to fibronectin (Fig. 8*C*).

Adhesion Defects in *Hox5* Triple-Mutant Fibroblasts Are Due to Loss of Itgα5/Itgβ1 Dimer Formation. Integrins play critical roles in cell adhesion by attaching the cell cytoskeleton to ECM substrates. We, therefore, analyzed the protein levels of several integrins with reported expression in the distal lung by Western analyses (46–51). We observed no changes in ItgaV, Itgb6, and Itga6 (Fig. 9*A*). However, striking decreases were measured in the levels of Itgα5 and its obligate heterodimer Itgβ1, an integrin dimer that has been defined as the initiating dimer responsible for fibronectin attachment, in *Hox5* conditional mutants compared with controls (Fig. 9*A*). Itga5 expression is also clearly reduced in the distal lung tissue in vivo when examined by IHC-IF (Fig. 9*B*). Isolation of *Hox5* mutant fibroblasts in cell culture also exhibits reduced Itga5 expression compared with controls, showing that this reduction is the fibroblast population (Fig. 9*C*). Despite the striking reduction of levels of Itga5/Itgb1 protein, qPCR measures no differences in the expression levels of any integrin candidate analyzed in *Hox5* mutants (*SI Appendix*, Fig. S7), including Itga5 and Itgb1, and indicates that *Hox5* genes do not likely directly regulate the expression of these integrins at the transcriptional level.

To determine whether reduction of the Itgα5/Itgβ1 dimer formation is sufficient to cause the observed reduction in adhesion in *Hox5* mutants, we performed in vitro blocking assays in which WT fibroblasts isolated from P7 lungs were allowed to adhere to fibronectin in the presence or absence of blocking antibodies for Itgα5, Itgβ1, or other integrins. Blocking with ItgaV, Itgb2, or an IgG control resulted in no changes in adhesion of lung fibroblasts to fibronectin-coated plates. However, blocking with Itgα5 or Itgβ1, alone or in combination, results in reductions in adherence to fibronectin that are similar to what we observe in our *Hox5* conditional mutant fibroblasts (Fig. 9*D*). Conditional *Hox5* triple-mutant fibroblasts exhibit a >35% reduction in adherence to fibronectin compared with an ∼46% reduction in fibronectin adherence when blocking Itgα5 and Itgβ1 in WT fibroblasts (compare Fig. 8*C* with Fig. 9*D*). Thus, blocking the adhesion by the Itgα5 and Itgβ1 integrins recapitulates the adhesion defect observed in *Hox5* triple-mutant fibroblasts.

Discussion

We have previously reported that all three *Hox5* genes (*Hoxa5*, *Hoxb5*, *Hoxc5*) are exclusively expressed in the lung mesenchyme (and not epithelium) during embryogenesis and that the most severe phenotypes result from the loss of function of all three *Hox5* genes (7). Because *Hox5* triple mutants die shortly after

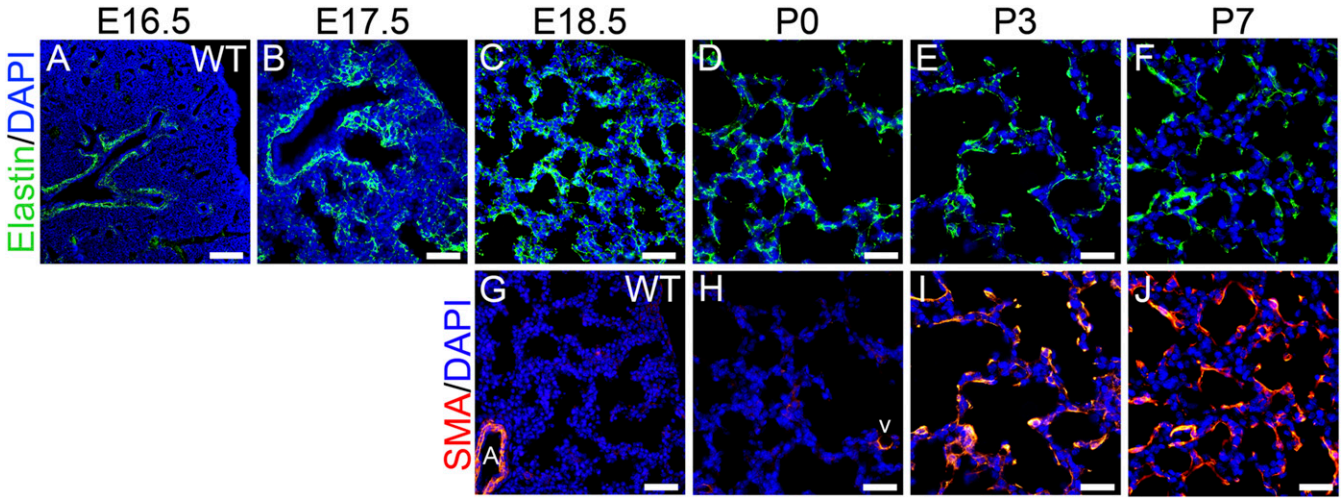

Fig. 6. Elastin and SMA expression time course in WT lungs. Elastin is exclusively expressed around the proximal airway through E16.5, with no expression detected in the distal airway (*A*). Elastin expression in the distal lung initiates at E17.5 (*B*), and a complex elastin network exists in the distal lung by E18.5 (*C*). The elastin network continues to be elaborated postbirth and is remodeled into more tightly organized elastin bundles located around the alveolar openings by P7 (*D*–*F*). No SMA+ myofibroblasts are observed in the distal lung until ∼P3 (*G*–*I*). By P7, SMA+ myofibroblasts form tight parallel networks with elastin (*F* and *J*). A, airway; V, vessel. (Scale bars: 50 μm.)

birth, previous studies have analyzed surviving compound mutants and determined that these genes continue to play important roles during postnatal development (18, 21, 32, 33, 52). To further address potential roles for all three *Hox5* genes during alveolar development, we generated a conditional allele for *Hoxa5* to use in combination with our existing null alleles for *Hoxb5* and *Hoxc5*. We show that early embryonic deletion of *Hoxa5* in an *Hoxb5*/*Hoxc5* double-mutant background fully recapitulates the previously reported lung phenotypes of the *Hox5* triple null animals (7). Additionally, we show that conditional loss of function of *Hoxa5* alone in the lung mesenchyme during early postnatal stages results in alveologenesis defects as previously reported (18). However, the degree of alveolar simplification observed in *Hox5* conditional triple mutants exceeds any combination of *Hoxa5* conditional/null alleles and shows the contribution of all three *Hox5* genes to alveologenesis. In addition, since the *Tbx4rtTA*;*TetOCre* allele exclusively deletes in the lung mesenchyme, our data provide strong support that the mesodermally derived lung fibroblasts are the primary drivers of elastogenesis during early postnatal stages.

The precise organization of the alveolar ECM is essential for proper alveolar development (40–45). Our data show no differences in the formation of any of the alveolar ECM components in conditional *Hox5* mutants except for disruption of the elastin matrix. Elastin null mice exhibit dilated saccules at birth due to a defect in primary septae formation, consistent with the critical role for elastin in alveolar development (43). Mice with loss-of-function mutations in various components of the elastogenesis pathway also result in alveolar simplification (reviewed in ref. 42). As the elastin matrix is generated by alveolar fibroblasts, the loss of integrity of the elastin network resulting from the deletion of *Hox5* function in the lung fibroblasts using the *Tbx4rtTA*;*TetOCre* allele indicates the critical role that these genes play within the fibroblast to direct proper alveologenesis. Interestingly, while the elastin-based ECM is highly disrupted in conditional *Hox5* triple mutants, Western analyses determined that levels of soluble elastin protein are unchanged. Hence, the irregular elastin network in *Hox5* mutants likely results from the inability to properly organize and/or remodel the elastin network during peak stages of alveologenesis and is not due to a lack of elastin protein production.

SMA+ fibroblasts of *Hox5* conditional triple mutants are morphologically abnormal and are unable to properly adhere to fibronectin. Given the importance of cell adhesion in this process, we analyzed several integrin candidates and identified significant decreases specifically in the levels of Itgα5 and Itgβ1. While Itgβ1 is promiscuous, Itgα5 only dimerizes with Itgβ1, forming an important heterodimer that is a major fibronectin receptor on a variety of cells, including human and mouse lung fibroblasts, and is sufficient to induce cell attachment and spreading (53–58). Consistent with these data, we find that using antibodies to individually or collectively block Itgα5 and Itgβ1 on WT fibroblasts reduces their ability to adhere to fibronectin and provides evidence that inhibition of this heterodimer is sufficient to recapitulate the adhesion defect observed in *Hox5* triple-mutant fibroblasts. Itga5 null mice are embryonic lethal; however, it has been shown that Itga5 promotes cell adhesion and migration on fibronectin, and elevation of ITGA5 in primary human lung fibroblasts has been linked to increased cell attachment to fibronectin (59–61). In a similar fashion, loss of integrin β1 in adult fibroblasts reduced their ability to adhere and spread on fibronectin (62). Thus, these data collectively support a model where *Hox5* genes play a critical role in fibroblast adhesion by regulating the levels of Itgα5/β1.

Many previous studies have found an association between *Hox* genes and integrins; however, most of the data supporting this relationship have been obtained in cell culture and are not related to a specific phenotype in vivo (63–70). However, one previous publication in *Hox* mutants reports that the kidney phenotypes resulting from loss of function of *Hoxa11*/*d11* are strikingly similar to those observed in *Integrin α8* mutant mice, and *Hoxa11*/*Hoxd11* mutant kidneys showed a reduction of *Integrin α8* expression (71). Despite the dramatic decrease in protein levels of Itga5/b1 in *Hox5* triple mutants, qPCR analyses show no differences in the expression levels of either of these genes and suggest that *Itga5* and *Itgb1* are not direct downstream targets of *Hox5*. It remains to be determined if *Hox* regulation of cell adhesion through integrins could be a general mechanism used by *Hox* genes to regulate morphogenetic behavior in vivo.

Collectively, our data highlight a continuing role for all three *Hox5* genes during postnatal alveologenesis. In this final phase of lung development, *Hox5* gene function is required for elastin network formation by regulating the adherence of the alveolar

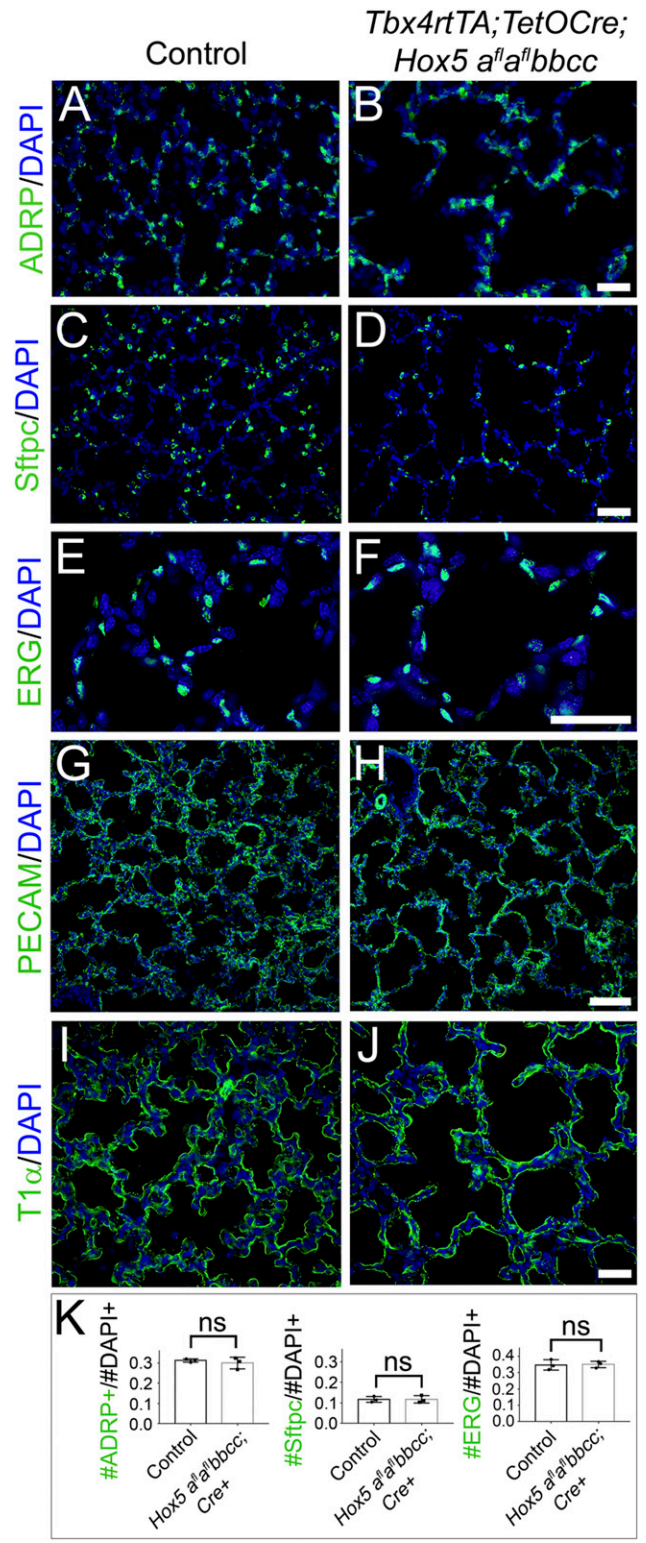

Fig. 7. Distribution of major cell types in the distal lung is unaffected in *Hox5* triple mutants at P7. The number and distribution of ADRP+ lipofibroblasts (*A* and *B*), Sftpc+ AECII cells (*C* and *D*), and ERG+ endothelial cells (*E* and *F*) are unaffected in *Hox5* triple mutants. No changes in PECAM+ endothelial (*G* and *H*) or T1α+ AECI cells (*I* and *J*) are observed in *Hox5* triple mutants at P7. (Scale bars: 50 μm.) Quantification (proportion of total DAPI+ cells) shows no differences in ratios of ADRP+, Sftpc+, or ERG+ cells in *Hox5* triple mutants (*K*). ns, not significant (*K*).

fibroblasts to the distal lung ECM. Additionally, we show that the disrupted elastin network leads to dramatic consequences in alveolar development that persist into adulthood and lead to severe physiological pathologies, including BPD-like symptoms of increased lung volume/compliance and decreased elastance. It will, therefore, be critical that future studies focus on better defining direct downstream mechanisms controlling these processes. The relationship between lung fibroblasts, elastin deposition, remodeling, and maintenance during early stages of alveologenesis will better inform strategies to treat lung disease.

Materials and Methods

Generation of Hoxa5 Conditional Mice. Single-guide (sgRNA) sequences targeting the introns immediately up- and downstream of exon2 of *Hoxa5* were designed and cloned into the pT7-Guide Vector (Blue Heron Biotech, LLC). Both the sequences and approximate location of the $n = 2$ sgRNAs are illustrated in Fig. 1*B*; in vitro transcription of sgRNAs from the pT7-Guide Vector was generated using the MEGAshortscript T7 kit (Life Technologies) and subsequently purified using the MEGAclear kit (Life Technologies). Cas9 mRNA was generated using the pT7-Cas9-nuclease vector (gift from Moisés Mallo, Instituto Gulbenkian de Ciencia, Oeiras, Portugal) using the mMESSAGE mMACHINE T7 ULTRA kit (Life Technologies) and purified using the MEGAclear kit (Life Technologies). Details on the production of

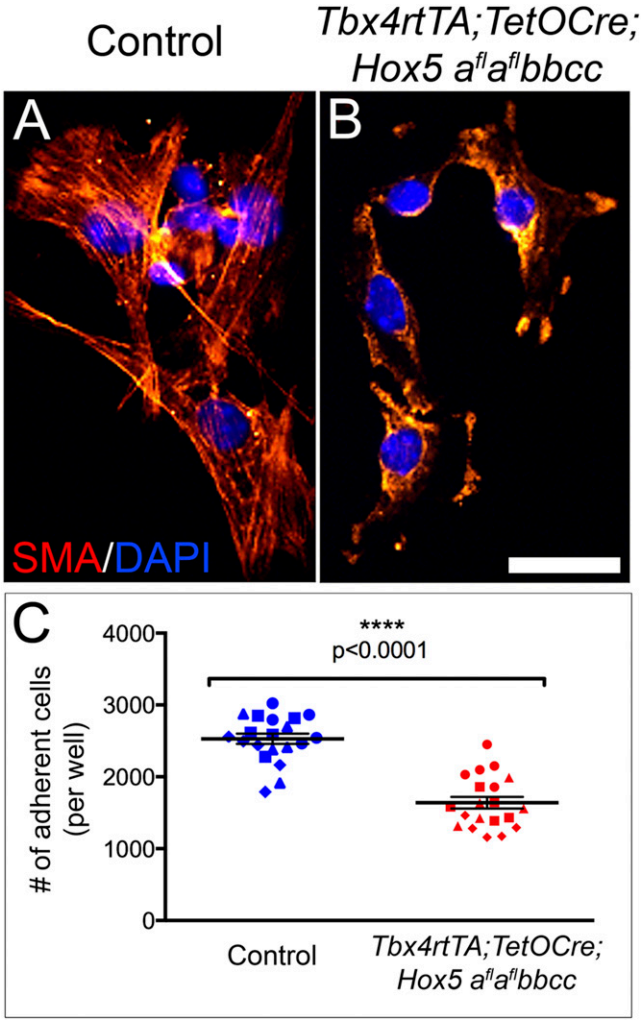

Fig. 8. SMA+ fibroblasts from *Hox5* triple mutants have severely abnormal morphology and lack the normal extended cell bodies observed in controls in vitro (*A* and *B*). (Scale bar: 25 μm.) In vitro adhesion assays show that fibroblasts isolated from *Hox5* triple mutants at P7 exhibit a significant reduction in their ability to adhere to fibronectin (*C*). Asterisks denote statistical significance (*C*).

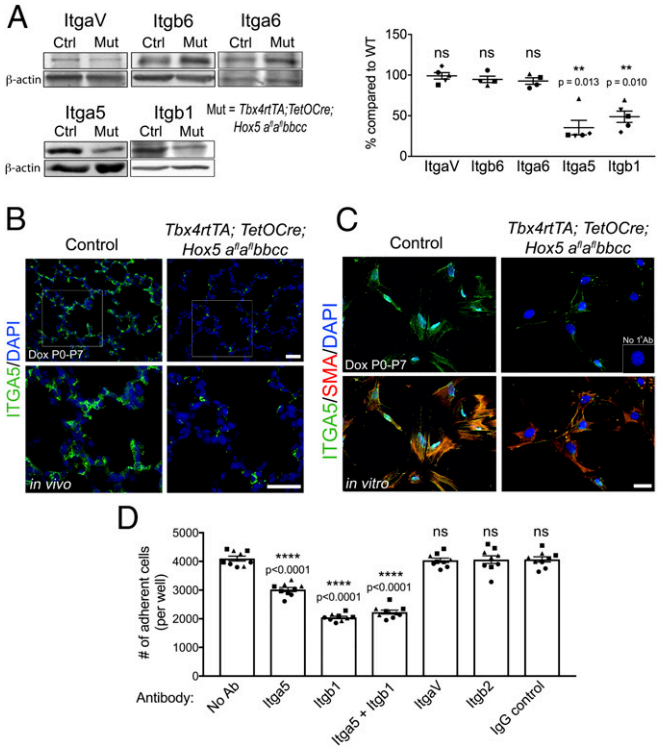

Fig. 9. Analysis of integrins in *Hox5* triple mutants at P7. Western analysis shows no difference in protein levels of ItgaV, Itgb6, or Itga6 in *Hox5* triple mutants compared with controls; however, there is a dramatic reduction in Itga5 and its obligate dimer Itgb1. Quantification of results confirms no changes in protein levels of ItgaV, Itgb6, or Itga6 but statistically significant differences in levels of Itga5 and Itgb1 (*A*). In vivo expression of Itga5 is dramatically reduced throughout the distal lung of *Hox5* triple mutants compared with controls at P7 (*B*). Itga5 immunohistochemistry in *Hox5* triple-mutant fibroblasts harvested at P7 (Dox from P0 to P7) reveals a dramatic reduction of Itga5 expression in SMA+ myofibroblasts in vitro compared with controls (*C*). (Scale bars: 50 μm.) In vitro adhesion assays were performed on WT fibroblasts harvested at P7 in the presence of blocking antibodies. Blocking with ItgaV and Itgb2 antibodies results in no changes in the ability of the fibroblasts to adhere to fibronectin, but using blocking antibodies Itga5 or Itgb1 (alone or together) results in decreased adherence (*D*). Asterisks denote statistical significance; ns, not significant (*D*).

oligonucleotide repair templates and zygote injection and confirmation of targeting are provided in *SI Appendix, SI Materials and Methods*. All other mice used in this study have been previously described, including the Hoxb5/c5 null mice (7, 10), Tbx4rtTA;TetOCre mice (34), and β-cat Flox (ctnnb1^{TM2Kem}) mice (72). All experiments were performed following protocols approved by the University of Michigan's Institutional Committee on the Use and Care of Animals.

Histology and Chord Length Measurements. Dissection, inflation, and fixation of postnatal lungs were performed as previously reported (33). Lungs were vacuum embedded in paraffin, sectioned at 5 μm, and stained with H&E. Mean alveolar chord length was determined as previously described (73).

Pulmonary Function Testing. Pulmonary function testing (PFT) analyses were performed in anesthetized mice after the insertion of a tracheal tube for mechanical breathing as previously described (33). In this study, P0–P14 Dox-treated 10-wk-old adult *Hox5 AABbCc* (control) and *Tbx4rtTA;TetOCre; Hoxa5^{fl}a^{fl}bbcc* (conditional *Hox5* triple mutant) animals were measured at baseline for changes in lung function. Statistical analyses were performed using unpaired Student's *t* test (GraphPad Prism software), and *P* values less than 0.05 were considered significant.

Immunohistochemistry and 3D Imaging. Immunohistochemistry protocols performed on 7-μm paraffin and frozen fixed sections have been previously described (7, 33). A complete list of all primary antibodies used in this study is provided in *SI Appendix*, Table S1. Tissue inflation and fixation for 100-μm-thick vibratome sections were prepared as previously reported (33); 3D reconstructions and movies were generated using IMARIS software (Bitplane).

Western Blot Analysis. Briefly, tissues were lysed in radioimmunoprecipitation assay buffer (50 mM Tris·HCl, pH 7.2, 150 mM NaCl, 0.1% Triton X-100, 1% sodium deoxycholate, 5 mM EDTA) containing Complete Mini Protease Inhibitor Mixture (Roche), and extracts were cleared by centrifugation at 20,000 × *g* for 30 min at 4 °C. Total protein content was assessed using the Pierce BCA protein assay kit (Thermo Scientific) and analyzed by SDS/PAGE after boiling in Laemmli sample buffer. Proteins were transferred to low-fluorescence polyvinylidene fluoride (GE Healthcare), blocked in 3% BSA with sodium azide, and probed with primary antibodies as indicated in *SI Appendix*, Table S1 and Alexa Fluor secondary antibodies (Invitrogen), which were diluted at 1:5,000. Fluorescence signals were detected on an Azure imaging system (Azure Biosystems). Western blot densitometry analysis was quantified using ImageJ.

Lung Fibroblast Isolation and Primary Culture. After isolation from animals, the trachea and proximal airway were removed from lungs by manual dissection and then rinsed in sterile PBS (Gibco). The remaining distal lung was then finely minced using a sterile scalpel and digested in a 10-mL solution containing 2 mg/mL Collagenase 1 and 3 mg/mL Dispase (Roche) in PBS for 2 h at 37 °C with shaking at 20-min intervals. The resulting cell suspension was added to 15 mL of DMEM/F12 (Invitrogen) supplemented with 10% FBS (Sigma) and 100 U/mL penicillin/streptomycin (Sigma) containing EDTA. Cells were briefly chilled on ice, incubated with erythrocyte lysis buffer, and then filtered through a 100-μm nylon cell strainer (Falcon, Becton, Dickinson and Company). Cells were washed twice in fresh DMEM and plated in six-well tissue culture-treated plates (Denville) at a density of 300,000 cells per well. Cells were maintained in medium consisting of DMEM/F12 (Invitrogen) supplemented with 10% FBS (Sigma) and 100 U/mL penicillin/streptomycin (Sigma); medium was changed every 3 d.

Adhesion Assays. Assay was performed as previously described (74). Details of the protocol are provided in *SI Appendix, SI Materials and Methods*. Antibodies used for blocking assays are included in *SI Appendix*, Table S1.

RNA Isolation and qRT-PCR. RNA was isolated from dissected distal pieces of postnatal and adult mouse lungs with the Qiagen RNeasy Micro Kit. qRT-PCR was performed and statistically analyzed as previously described (7). qPCR primer sequences for all three *Hox5* genes have been previously reported (7). All other qPCR primers used in this study are listed in *SI Appendix*, Table S2.

TEM. The left lobes of the lungs of control and *Hox5* triple mutants were prepared for TEM imaging as previously described (75) with slight modifications. A detailed TEM protocol is provided in *SI Appendix, SI Materials and Methods*. Images were captured using a JEOL JEM 1400 –+ transmission electron microscope.

ACKNOWLEDGMENTS. We thank N. D'Silva for providing the antibodies and technical expertise for the adhesion assays with blocking antibodies. We also thank Jeff Harrison (University of Michigan Microscopy and Imaging Analysis Laboratory) for his assistance in TEM preparation and imaging. We acknowledge Wanda Filipiak and Galina Gavrilina for preparation of transgenic mice and the Transgenic Animal Model Core of the University of Michigan's Biomedical Research Core Facilities. This work was supported by Ruth L. Kirschstein National Research Service Award Training Grant 5 T32 HL 7749-20 (to S.M.H.). This research was also supported by Michigan Institute for Clinical and Health Research Postdoctoral Translational Scholars Program Grant UL1TR002240 (to L.M.-S.) and National Heart, Lung, and Blood Institute Grant R01-HL119215 (to D.M.W.). Core support was provided by the University of Michigan George M. O'Brien Renal Core Center through NIH Grant P30DK08194. Research reported in this publication was supported by National Cancer Institute of the NIH Award P30CA046592.

1. Kessel M, Gruss P (1990) Murine developmental control genes. *Science* 249:374–379.
2. Chen F, Capecchi MR (1997) Targeted mutations in hoxa-9 and hoxb-9 reveal synergistic interactions. *Dev Biol* 181:186–196.
3. Chen F, Capecchi MR (1999) Paralogous mouse Hox genes, Hoxa9, Hoxb9, and Hoxd9, function together to control development of the mammary gland in response to pregnancy. *Proc Natl Acad Sci USA* 96:541–546.
4. Davis AP, Witte DP, Hsieh-Li HM, Potter SS, Capecchi MR (1995) Absence of radius and ulna in mice lacking hoxa-11 and hoxd-11. *Nature* 375:791–795.
5. Fromental-Ramain C, et al. (1996) Specific and redundant functions of the paralogous Hoxa-9 and Hoxd-9 genes in forelimb and axial skeleton patterning. *Development* 122:461–472.
6. Fromental-Ramain C, et al. (1996) Hoxa-13 and Hoxd-13 play a crucial role in the patterning of the limb autopod. *Development* 122:2997–3011.

DEVELOPMENTAL BIOLOGY

7. Hrycaj SM, et al. (2015) Hox5 genes regulate the Wnt2/2b-Bmp4-signaling axis during lung development. *Cell Rep* 12:903–912.
8. Larsen BM, Hrycaj SM, Newman M, Li Y, Wellik DM (2015) Mesenchymal Hox6 function is required for mouse pancreatic endocrine cell differentiation. *Development* 142: 3859–3868.
9. Manley NR, Capecchi MR (1998) Hox group 3 paralogs regulate the development and migration of the thymus, thyroid, and parathyroid glands. *Dev Biol* 195:1–15.
10. McIntyre DC, et al. (2007) Hox patterning of the vertebrate rib cage. *Development* 134:2981–2989.
11. Rossel M, Capecchi MR (1999) Mice mutant for both Hoxa1 and Hoxb1 show extensive remodeling of the hindbrain and defects in craniofacial development. *Development* 126:5027–5040.
12. van den Akker E, et al. (2001) Axial skeletal patterning in mice lacking all paralogous group 8 Hox genes. *Development* 128:1911–1921.
13. Wellik DM, Capecchi MR (2003) Hox10 and Hox11 genes are required to globally pattern the mammalian skeleton. *Science* 301:363–367.
14. Wellik DM, Hawkes PJ, Capecchi MR (2002) Hox11 paralogous genes are essential for metanephric kidney induction. *Genes Dev* 16:1423–1432.
15. Xu B, et al. (2013) Hox5 interacts with Plzf to restrict Shh expression in the developing forelimb. *Proc Natl Acad Sci USA* 110:19438–19443.
16. Xu B, Wellik DM (2011) Axial Hox9 activity establishes the posterior field in the developing forelimb. *Proc Natl Acad Sci USA* 108:4888–4891.
17. Leucht P, et al. (2008) Embryonic origin and Hox status determine progenitor cell fate during adult bone regeneration. *Development* 135:2845–2854.
18. Mandeville I, et al. (2006) Impact of the loss of Hoxa5 function on lung alveogenesis. *Am J Pathol* 169:1312–1327.
19. Papagiannouli F, Schardt L, Grajcarek J, Ha N, Lohmann I (2014) The Hox gene Abd-B controls stem cell niche function in the Drosophila testis. *Dev Cell* 28:189–202.
20. Pineault KM, et al. (2015) Hox11 genes regulate postnatal longitudinal bone growth and growth plate proliferation. *Biol Open* 4:1538–1548.
21. Ptaschinski C, Hrycaj SM, Schaller MA, Wellik DM, Lukacs NW (2017) *Hox5* paralogous genes modulate Th2 cell function during chronic allergic inflammation via regulation of *Gata3*. *J Immunol* 199:501–509.
22. Rinn JL, et al. (2008) A dermal HOX transcriptional program regulates site-specific epidermal fate. *Genes Dev* 22:303–307.
23. Rux DR, et al. (2017) Hox11 function is required for region-specific fracture repair. *J Bone Miner Res* 32:1750–1760.
24. Rux DR, et al. (2016) Regionally restricted hox function in adult bone marrow multipotent mesenchymal stem/stromal cells. *Dev Cell* 39:653–666.
25. Stultz BG, Park SY, Mortin MA, Kennison JA, Hursh DA (2012) Hox proteins coordinate peripodial decapentaplegic expression to direct adult head morphogenesis in Drosophila. *Dev Biol* 369:362–376.
26. Chisaka O, Capecchi MR (1991) Regionally restricted developmental defects resulting from targeted disruption of the mouse homeobox gene hox-1.5. *Nature* 350:473–479.
27. Davenne M, et al. (1999) Hoxa2 and Hoxb2 control dorsoventral patterns of neuronal development in the rostral hindbrain. *Neuron* 22:677–691.
28. Horan GS, et al. (1995) Compound mutants for the paralogous hoxa-4, hoxb-4, and hoxd-4 genes show more complete homeotic transformations and a dose-dependent increase in the number of vertebrae transformed. *Genes Dev* 9:1667–1677.
29. Lufkin T, Dierich A, LeMeur M, Mark M, Chambon P (1991) Disruption of the Hox-1.6 homeobox gene results in defects in a region corresponding to its rostral domain of expression. *Cell* 66:1105–1119.
30. Yallowitz AR, Hrycaj SM, Short KM, Smyth IM, Wellik DM (2011) Hox10 genes function in kidney development in the differentiation and integration of the cortical stroma. *PLoS One* 6:e23410.
31. Branchfield K, et al. (2016) A three-dimensional study of alveologenesis in mouse lung. *Dev Biol* 409:429–441.
32. Aubin J, Lemieux M, Tremblay M, Bérard J, Jeannotte L (1997) Early postnatal lethality in Hoxa-5 mutant mice is attributable to respiratory tract defects. *Dev Biol* 192: 432–445.
33. Hrycaj SM, Marty-Santos L, Rasky AJ, Lukacs NW, Wellik DM (April 27, 2018) Loss of Hox5 function results in myofibroblast mislocalization and distal lung matrix defects during postnatal development. *Sci China Life Sci*, 10.1007/s11427-017-9290-1.
34. Zhang W, et al. (2013) Spatial-temporal targeting of lung-specific mesenchyme by a Tbx4 enhancer. *BMC Biol* 11:111.
35. Ventura A, et al. (2007) Restoration of p53 function leads to tumour regression in vivo. *Nature* 445:661–665.
36. Mund SI, Stampanoni M, Schittny JC (2008) Developmental alveolarization of the mouse lung. *Dev Dyn* 237:2108–2116.
37. Schittny JC, Mund SI, Stampanoni M (2008) Evidence and structural mechanism for late lung alveolarization. *Am J Physiol Lung Cell Mol Physiol* 294:L246–L254.
38. Madisen L, et al. (2010) A robust and high-throughput Cre reporting and characterization system for the whole mouse brain. *Nat Neurosci* 13:133–140.
39. Frank DB, et al. (2016) Emergence of a wave of Wnt signaling that regulates lung alveologenesis by controlling epithelial self-renewal and differentiation. *Cell Rep* 17: 2312–2325.
40. Li R, Herriges JC, Chen L, Mecham RP, Sun X (2017) FGF receptors control alveolar elastogenesis. *Development* 144:4563–4572.
41. Neptune ER, et al. (2003) Dysregulation of TGF-beta activation contributes to pathogenesis in Marfan syndrome. *Nat Genet* 33:407–411.
42. Wagenseil JE, Mecham RP (2007) New insights into elastic fiber assembly. *Birth Defects Res C Embryo Today* 81:229–240.
43. Wendel DP, Taylor DG, Albertine KH, Keating MT, Li DY (2000) Impaired distal airway development in mice lacking elastin. *Am J Respir Cell Mol Biol* 23:320–326.
44. Yanagisawa H, Schluterman MK, Brekken RA (2009) Fibulin-5, an integrin-binding matricellular protein: Its function in development and disease. *J Cell Commun Signal* 3:337–347.
45. Yeo GC, Keeley FW, Weiss AS (2011) Coacervation of tropoelastin. *Adv Colloid Interface Sci* 167:94–103.
46. Horan GS, et al. (2008) Partial inhibition of integrin alpha(v)beta6 prevents pulmonary fibrosis without exacerbating inflammation. *Am J Respir Crit Care Med* 177: 56–65.
47. Tatler AL, et al. (2016) Amplification of TGFβ induced ITGB6 gene transcription may promote pulmonary fibrosis. *PLoS One* 11:e0158047.
48. Chen H, et al. (2005) Abnormal mouse lung alveolarization caused by Smad3 deficiency is a developmental antecedent of centrilobular emphysema. *Am J Physiol Lung Cell Mol Physiol* 288:L683–L691.
49. Terpe HJ, Stark H, Ruiz P, Imhof BA (1994) Alpha 6 integrin distribution in human embryonic and adult tissues. *Histochemistry* 101:41–49.
50. Munger JS, et al. (1999) The integrin alpha v beta 6 binds and activates latent TGF beta 1: A mechanism for regulating pulmonary inflammation and fibrosis. *Cell* 96: 319–328.
51. Singh B, Fu C, Bhattacharya J (2000) Vascular expression of the alpha(v)beta(3)-integrin in lung and other organs. *Am J Physiol Lung Cell Mol Physiol* 278:L217–L226.
52. Boucherat O, et al. (2013) Partial functional redundancy between Hoxa5 and Hoxb5 paralog genes during lung morphogenesis. *Am J Physiol Lung Cell Mol Physiol* 304:L817–L830.
53. Nagae M, et al. (2012) Crystal structure of α5β1 integrin ectodomain: Atomic details of the fibronectin receptor. *J Cell Biol* 197:131–140.
54. Obara M, Kang MS, Yamada KM (1988) Site-directed mutagenesis of the cell-binding domain of human fibronectin: Separable, synergistic sites mediate adhesive function. *Cell* 53:649–657.
55. Schaffner F, Ray AM, Dontenwill M (2013) Integrin α5β1, the fibronectin receptor, as a pertinent therapeutic target in solid tumors. *Cancers (Basel)* 5:27–47.
56. White ES, et al. (2003) Integrin alpha4beta1 regulates migration across basement membranes by lung fibroblasts: A role for phosphatase and tensin homologue deleted on chromosome 10. *Am J Respir Crit Care Med* 168:436–442.
57. Dalton SL, Marcantonio EE, Assoian RK (1992) Cell attachment controls fibronectin and alpha 5 beta 1 integrin levels in fibroblasts. Implications for anchorage-dependent and -independent growth. *J Biol Chem* 267:8186–8191.
58. Ingber DE (1990) Fibronectin controls capillary endothelial cell growth by modulating cell shape. *Proc Natl Acad Sci USA* 87:3579–3583.
59. Wang QY, Zhang Y, Shen ZH, Chen HL (2008) alpha1,3 fucosyltransferase-VII upregulates the mRNA of alpha5 integrin and its biological function. *J Cell Biochem* 104:2078–2090.
60. Epstein Shochet G, Brook E, Israeli-Shani L, Edelstein E, Shitrit D (2017) Fibroblast paracrine TNF-α signaling elevates integrin A5 expression in idiopathic pulmonary fibrosis (IPF). *Respir Res* 18:122.
61. Watt FM, Hodivala KJ (1994) Cell adhesion. Fibronectin and integrin knockouts come unstuck. *Curr Biol* 4:270–272.
62. Liu S, et al. (2010) Expression of integrin beta1 by fibroblasts is required for tissue repair in vivo. *J Cell Sci* 123:3674–3682.
63. Hamada Ji, et al. (2001) Overexpression of homeobox gene HOXD3 induces coordinate expression of metastasis-related genes in human lung cancer cells. *Int J Cancer* 93:516–525.
64. Ohta H, et al. (2006) HOXD3-overexpression increases integrin alpha v beta 3 expression and deprives E-cadherin while it enhances cell motility in A549 cells. *Clin Exp Metastasis* 23:381–390.
65. Boudreau NJ, Varner JA (2004) The homeobox transcription factor Hox D3 promotes integrin alpha5beta1 expression and function during angiogenesis. *J Biol Chem* 279: 4862–4868.
66. Myers C, Charboneau A, Boudreau N (2000) Homeobox B3 promotes capillary morphogenesis and angiogenesis. *J Cell Biol* 148:343–351.
67. Bei L, et al. (2007) Identification of a HoxA10 activation domain necessary for transcription of the gene encoding beta3 integrin during myeloid differentiation. *J Biol Chem* 282:16846–16859.
68. Daftary GS, Troy PJ, Bagot CN, Young SL, Taylor HS (2002) Direct regulation of beta3-integrin subunit gene expression by HOXA10 in endometrial cells. *Mol Endocrinol* 16: 571–579.
69. Klausen C, Leung PC, Auersperg N (2009) Cell motility and spreading are suppressed by HOXA4 in ovarian cancer cells: Possible involvement of beta1 integrin. *Mol Cancer Res* 7:1425–1437.
70. Park H, et al. (2011) Homeobox D1 regulates angiogenic functions of endothelial cells via integrin β1 expression. *Biochem Biophys Res Commun* 408:186–192.
71. Valerius MT, Patterson LT, Feng Y, Potter SS (2002) Hoxa 11 is upstream of Integrin alpha8 expression in the developing kidney. *Proc Natl Acad Sci USA* 99:8090–8095.
72. Brault V, et al. (2001) Inactivation of the beta-catenin gene by Wnt1-Cre-mediated deletion results in dramatic brain malformation and failure of craniofacial development. *Development* 128:1253–1264.
73. Sajjan U, et al. (2009) Elastase- and LPS-exposed mice display altered responses to rhinovirus infection. *Am J Physiol Lung Cell Mol Physiol* 297:L931–L944.
74. Kohan M, Muro AF, White ES, Berkman N (2010) EDA-containing cellular fibronectin induces fibroblast differentiation through binding to alpha4beta7 integrin receptor and MAPK/Erk 1/2-dependent signaling. *FASEB J* 24:4503–4512.
75. Dabovic B, et al. (2009) Dual functions for LTBP in lung development: LTBP-4 independently modulates elastogenesis and TGF-beta activity. *J Cell Physiol* 219:14–22.